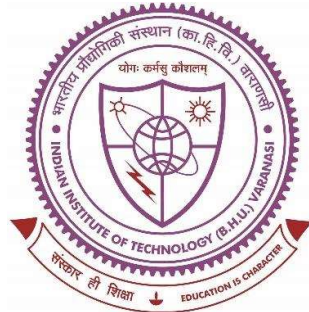


**DESIGN OF CHAIN PILLARS FOR DEEP LONGWALL WORKINGS IN
INDIAN GEO-MINING CONDITIONS**



Thesis submitted in partial fulfilment for the Award of Degree

Doctor of Philosophy

By

AJEET YADAV

DEPARTMENT OF MINING ENGINEERING

INDIAN INSTITUTE OF TECHNOLOGY

(BANARAS HINDU UNIVERSITY)

VARANASI-221005

ROLL.NO – 16151002

YEAR OF SUBMISSION – 2022

CERTIFICATE

It is certified that the work contained in the thesis titled "*DESIGN OF CHAIN PILLARS FOR DEEP LONGWALL WORKINGS IN INDIAN GEO-MINING CONDITIONS*" has been carried out under our supervision and that this work has not been submitted elsewhere for a degree.

It is further certified that the student has fulfilled all the requirements of Comprehensive Examination, Candidacy and SOTA for the award of Ph.D. Degree.



Supervisor
Dr. G.S.P. Singh
(Associate professor)

DECLARATION BY THE CANDIDATE

I, "AJEET YADAV", certify that the work embodied in this thesis is my own bona fide work and carried out by me under the supervision of "Dr. G.S.P. SINGH" from "JULY 2016" to "JULY 2022", at the "DEPARTMENT OF MINING ENGINEERING", Indian Institute of Technology (B.H.U), Varanasi. The matter embodied in this thesis has not been submitted for the award of any other degree/diploma. I declare that I have faithfully acknowledged and given credits to the research workers wherever their works have been cited in my work in this thesis. I further declare that I have not willfully copied any other's work, paragraphs, text, data, results, etc., reported in journals, books, magazines, reports dissertations, theses, etc., or available at websites and have not included them in this thesis and have not cited as my own work.

Date: 04.07.2022

Place: Varanasi

Ajeet Yadav
(AJEET YADAV)

CERTIFICATE BY THE SUPERVISOR

It is certified that the above statement made by the student is correct to the best of our knowledge.



Supervisor

Dr. G.S.P. Singh
(Associate professor)

Dr. G.S.P. Singh
04/07/2022

Signature of Head of Department/Coordinator of School
"SEAL OF THE DEPARTMENT/SCHOOL"

DEPT. OF MINING ENGG.
भारतीय प्रौद्योगिकी संस्थान (भारतीय प्रौद्योगिकी संस्थान)
Indian Institute of Technology (Indian Institute of Technology)
वाराणसी-221005

COPYRIGHT TRANSFER CERTIFICATE

Title of the Thesis: Design of Chain Pillars for Deep Longwall Workings in Indian Geo-Mining Conditions.

Name of the Student: AJEET YADAV

Copyright Transfer

The undersigned hereby assigns to the Indian Institute of Technology (Banaras Hindu University) Varanasi all rights under copyright that may exist in and for the above thesis submitted for the award of the "*Doctor of Philosophy*".

Date: 04.07.2022

Place: Varanasi

Ajeet Yadav

(AJEET YADAV)

Note: However, the author may reproduce or authorise others to reproduce material extracted verbatim from the thesis or derivative of the thesis for author's personal use provided that the source and Institute's copyright notice are indicated.

ACKNOWLEDGEMENT

Words cannot express my gratitude to my supervisor, Dr. G.S.P. Singh for his invaluable patience and feedback. I cannot overemphasize his contributions in my life as a researcher and also as a person. He allowed me to grow as a researcher under his invaluable guidance.

I have been incredibly grateful for the support and feedback given by my thesis committee members: Prof. Sanjay. K. Sharma and Dr. P Bala Ramadu. I am also grateful to Prof. Sanjay. K. Sharma for his support and motivating words. I would also like to extend my sincere thanks to Prof. Pramod K Jain, Director, IIT (B.H.U) Varanasi and Prof. Suprakash Gupta, Head, Department of the Mining engineering, for their support throughout the research work.

Special thanks to the management of BCCL, ECL, and SCCL for providing the necessary field data, which were essential inputs of this investigation. I am thankful to Mr. Sunny Rao, Deputy Manager, Moonidih Colliery, BCCL and Mr. Srikant, Strata Control Engineer, Adriyala Longwall Project, SCCL, for their cooperation and sharing valuable experiences.

I would like to thank my friends Mr. Ashutosh K. Bharati, Mr. Vijay Singh, Mr. Sandeep K. Prajapati, Mr. Samarjeet Kumar, and Mr. Pradeep K. Jangid for their unconditional support and love. They showed an immense believe in me and have been there like rock though my thick and thins.

Special thanks to Dr. Bhaskara Behera and Dr. Sandeep K. Sahoo, My seniors and most importantly a great friend. Thanks to Mr. Ankush Galav, Mr. Gagan Gupta, Mr. Anupam Chaturvedi, and Mr. Shiv Govind for their helping hand during the various challenging situations throughout this journey.

Last but not least, I would like to express my eternal gratitude to my parents, brother, and sisters for their continuous support and trust in me. I owe almost everything to them as this journey would not have been possible without their invaluable support. Their mere presence allowed me to carry out this research work without bothering much about my responsibilities.

Abstract

India is witnessing a significant increase in domestic energy demand due to its expanding economy, industrialisation, urbanisation, and population. The projected coal demand is likely to touch 1.5 billion tons in the country by 2030, which is 63% higher than the current demand level. The open-pit mining is staring at several challenges because of numerous reasons. Hence, the mining industry in the country is bound to shift its focus to underground mining to increase production and keep up with the projected future coal demand. Longwall mining is the most efficient mass production technology for the extraction of deep coal seams. Rational design of chain pillars is indispensable to ensure adequate isolation from the adjoining goaf and stability of gate roads for safe access and unhindered production from the longwall faces. In India, the design of chain pillars has not garnered much attention. They are mostly designed following the regulatory provisions for support pillars. The approach of chain pillar design for longwall workings should be different from the approach for the design of support pillars in Bord and Pillar workings because of the fundamental difference in the layout of pillars and their loading conditions. Chain pillars designed using such an approach are generally oversized, leading to a significant mineral loss. The global trend in longwall design is towards longer and wider panels. The design of such panels at high cover depth requires multiple entries to meet the ventilation requirement. Hence, the need is to design the chain pillars with adequate safety by accurately identifying the loading and strength conditions.

In consideration of these requirements, the objectives of the present work were to develop a numerical modelling-based approach for the design of abutment chain pillars for deep longwall workings, conduct a detailed parametric study to identify the critical factors affecting the failure mechanism and stability of the chain pillars, establish a safety factor based criterion for designing abutment chain pillars considering single and double-row layouts in Indian geo-mining conditions, and evaluate the performance of the approach through a few case studies.

The scope of the work was limited to the design of chain pillars with their functional objective of isolation of longwall panels at a cover depth exceeding 360 m. The design of the yielding type chain pillar is beyond the scope of this work.

The methodology used in this study consisted of review of pertinent literature for the estimation of chain pillar stability and considerations in chain pillar design, compilation and analysis of laboratory and field data related to geo-technical, geo-mining, and field experiences for a set of longwall workings in different coal fields in India, development of a modelling procedure to simulate the failure mechanics of the coal specimens and constitutive behaviour of the caved gob material at the laboratory scale, development of three-dimensional numerical modelling procedures to determine the abutment angle formed due to caving of the overlying strata with progressive face advance, development of plain-strain modelling procedures to determine the strength and deformation properties of the damaged overlying strata due to mining and to evaluate the chain pillar stability, development of modelling procedures for simulating failed and stable coal pillars cases and determining the factor of safety-based criterion for chain pillar stability, parametric study of factors affecting FoS of the chain pillars and the abutment angle, development of a standard approach for estimating the post-failure softening parameters of the coal pillars and abutment angle, development of a machine learning-based model to estimate the pillar stability, and verification of the developed approach through case studies.

The literature review covered the general understanding of stress redistribution and damage of overlying roof strata that lead to the different intensity and quantum of load transfer on the chain pillars in different geo-mining conditions. It also highlighted the design requirement of such structures based on theoretical understanding and field experiences. The state of the art of chain pillar design, their strengths and limitations were also highlighted in the context of deep longwall workings in Indian conditions. The study showed that although a significant knowledge base is available for characterising the post-failure behaviour and strength of the

pillars, further work was needed to estimate the overall behaviour for the optimal design of chain pillars. The work showed that the mechanical behaviour of the pillar was closely associated with its w/h ratio and confinement provided by contact surfaces, followed by post-failure softening and dilatancy of the material. Abutment angle was a critical parameter to be carefully assessed with due consideration of the depth of cover, length of the face, and mechanical properties of the overlying strata for a field representative understanding of the behaviour of the chain pillars in a given set of conditions. An appropriate understanding of the behaviour of the 'Caved', 'Fractured', and 'Continuous deformation' zones in the overlying strata was also crucial for consideration of different loading in subcritical and supercritical workings. The design criteria for deciding the size of the chain pillar were found to be highly sensitive to the strength estimation method. Hence, a thorough evaluation of a specific criterion over a field representative database of stable and failed pillars was required to develop reasonable confidence in its applicability. In the absence of any scientific approach for the design of chain pillars, particularly for deep workings, the prevailing practice is wholly based on site-specific field experiences.

Simulation of the Complete Stress-Strain Behaviour

The post-failure strength parameters for different coal seams were estimated by simulating the observed behaviour during the servo-controlled uniaxial tests in the laboratory for w/h ratio ranging from 0.5-13.5 for six coal seams pertaining to three different coalfields in India. The study considered 126 calibrated models (Model III) to develop a set of empirical relations for selecting post-failure strength parameters to simulate the strain-softening behaviour of the coal specimen for different w/h ratios. A reasonable estimate of the dilatancy properties and the properties of interfaces at the contact surfaces were also worked out for improved simulation of the post-failure behaviour.

The study confirmed that the pillars having a w/h ratio less than 2 had a brittle post-failure behaviour. In contrast, the pillars having w/h of 2-6 showed strain-softening behaviour, and those with w/h of 6-9 showed strain-softening behaviour followed by strain-hardening characteristics after attaining the residual strength because of the reconsolidation of the broken material around the core. The failure state and mobilisation of the interface at the contact planes in the roof-pillar-floor system also showed a similar behaviour as noted at the specimen scale. The pillar having w/h of 3.6 failed completely up to the core at the residual strength stage, but the slippage of the interface at the core zone was negligible. This observation was similar to the model observed results of the laboratory-scale specimen having a w/h of 4.5. The failed elements around the core and the interface effect enabled sufficient residual strength of the pillar. The pillar had a small elastic core at its peak strength. The failure at the mid-height of the pillar penetrated deeper than the failure at the contact surfaces of the roof-pillar-floor system.

The stress versus strain profile confirmed the transition of post-failure behaviour from strain-softening to ductile. The uniaxial compression test for this sample showed considerable dilation till w/h of 4.5. For the w/h ratio exceeding 7.7, the specimen showed strain-hardening behaviour with accelerated development of positive volumetric strain and an insignificant dilation during the axial loading. The plots of failure state and slippage of the interface at the contact surfaces established that the core of the specimens could hold their stability even after the failure of the ribs and slippage of the interface at these locations. However, the extent of slippage, as well as the failure, reduced with the increasing w/h ratio. Although the specimen having a w/h ratio of 4.5 showed complete failure during its uniaxial compression, the interface could hold its original position in the centre, helping the specimen retain its residual strength after failure. The plot of differential stress and volumetric strain also confirmed the closure of dilation as indicated by the positive volumetric strain in such specimens. The validation of the

modelling approach with the triaxial compression test reported by Medhurst (1996) indicated a very close agreement of the results with the laboratory findings. At low confinement, the samples received a typical hourglass pattern of failure, while it transitioned to the typical shear mode of failure in well-defined planes with the increasing confinement. The failure was uncontrolled at lower confinement, but it became gradual with increasing confinement.

Assessment of Caved Goaf Parameters

Model II considered the constitutive behaviour of the goaf material reported by Salamon (1990) and the laboratory test results of Pappas and Mark (1994) to develop a standard approach for deriving the model parameters of the Double yield material to simulate the site-specific behaviour of caved goaf in a given geo-mining condition. It simulated the confined uniaxial compression of the caved goaf material considering the initial modulus (E_0) of goaf material varying from 10-50 MPa and bulking factor ('b') of the material varying from 1.1-1.5 in a cylindrical chamber of 365 mm diameter and 305 mm height, as reported in the laboratory test. The Double yield model parameters were established in terms of density, maximum bulk and shear moduli, angle of internal friction, dilation angle, Poisson's ratio, and the multiplier 'R' associated with the cap pressure. The density of the goaf material was scaled down from the intact rock density considering the conservation of mass and the bulking factor of the goaf material formed upon the caving of the strata within the caving zone. The maximum bulk and shear moduli were estimated from the elastic modulus of the goaf material (Equation 6.6) using standard relation considering Poisson's ratio of 0.2.

Several experimental models were run to establish the relation between cap pressure and stress recovery for different values of E_0 and 'b'. A provisional estimate of the cap-pressure table was made using the Salamon (1990) model for the given value of E_0 and 'b' for maximum vertical stress anticipated at a given cover depth. The double yield material property, along with the

maximum bulk and shear moduli, were input into the numerical model of the confined uniaxial test to obtain the axial stress versus strain curve at the different stages of loading and compare it with the provisional cap-pressure table. It was observed that a constant ratio lies between the cap pressure and the stress-strain curve for a given set of goaf material properties. The derived ratio was used to obtain the final cap-pressure table for a given set of conditions.

Estimation of Abutment Angle

An in-depth parametric study was undertaken through three-dimensional numerical modelling (Model V) to evaluate the abutment angle that formed along the edge of the chain pillar for different caving profiles of the roof strata in different longwall panels at different depths of cover. The study considered cover depth varying from 350-900 m and thickness ratio of the strata within the Caved zone varying from 0.5 to 2.0 for the soft, moderate, and hard strata conditions. The strength properties of these strata were assigned utilising the database from 27 different longwall workings in different coalfields in India.

The study indicated variations in abutment angle from 1 to 70° for different strengths of the strata at the cover depth of 350-900 m and face length and thickness ratio of 150-250 m and 0.5-2.0, respectively. A statistical model was developed using the results of the 81 parametric numerical models to estimate the abutment angle as the function of cover depth, face length, strength, thickness, and unit weight of the roof layers in the Caved zone. The study showed that when the immediate and the main roof layers are of similar thickness and massive, the system of roof layers develops a poor bending tendency resulting in a low caving angle and a large abutment angle. However, when the thickness of the main roof is lower, it works as a loading layer for the thicker immediate roof resulting in increased bending of the immediate roof layer. The caving angle of the strata in such a case is higher, which produces a low abutment angle. When the thickness of the immediate roof is lower than the main roof, the

main roof does not act as the loading layer. Hence, the two layers undergo independent bending without influencing the bending tendency of the lower layer. Hence, the overall bending of the composite layer is of moderate nature, producing the resultant abutment angle in between the previous two conditions.

The abutment angle varied from 10 to 25° for the decrease in the face length from 250m to 150m at the cover depth of 600 m in the moderate strength condition of the strata with the thickness ratio of 1.0. With a change in the cover depth from 350 to 900 m, the abutment angle decreased from 38 to 5° for the moderate strength condition, face length of 200m, and thickness ratio of 1.0. However, the abutment angle increased from 8 to 32° for the strength changing from soft to hard at the cover depth of 600, face length of 200 m, and the thickness ratio of 1.0. At the cover depth of 600m, face length of 200m, and moderately strong strata condition, the maximum and the minimum abutment angle of 18° and 3° were observed for thickness ratios of 1.0 and 0.5, while the abutment angle was 7° for the thickness ratio of 2.0.

The verification of the model outcome through field observations (Das, 2000) confirmed a variable abutment angle under different geo-mining conditions in contrast to its constant value adopted in previous studies. The results were also consistent with the findings of Tulu and Heasley (2012), Hill et al. (2015), and Tuncay et al. (2021), explaining the influence of the cover depth and panel width on the abutment angle.

The Factor of Safety of the Chain Pillars

The modelling study of 23 failed, and 20 stable cases of support pillars were conducted using model IV, considering the control parameters of the post-failure behaviour of the pillars and the Sheorey's failure criterion for deriving the triaxial strength properties for different coal seams. The uniaxial compression test for all the cases was modelled considering the Mohr-Coulomb strain-softening (MCSS) failure criterion for coal and elastic material model for roof

and floor strata to quantify the failure strengths and distinguish failed and stable cases of the pillars based on their factor of safety (FoS). The study showed that almost all the cases of failed pillars had $FoS < 1$. The median safety factor for these cases was 0.78, which was subsequently opted as the criterion for the optimal design of chain pillars considering their ultimate loading stage.

Strength and Deformability Parameters of the Damaged Zones in the Overlying Strata

The Model VI considered the Caved zone of 15 times the extraction height, considering the worst possible bulking factor of 1.07 in Indian geo-mining conditions. Four numerical models were considered at the cover depth ranging from 50 to 74 m and face length of 120 to 150 m, representing panels 'W2' in RVII coal seam at Jhanjra mine, panel 'P1' in Passang coal seam at Balrampur, panel 'K5' in Passang coal seam at New Kumda, and panel 'P2' in Burhar VIB coal seam at Rajendra Colliery to simulate the expected surface subsidence in these conditions by seeking appropriate constitutive behaviour and material properties of the rock mass in the 'Fractured' zone that lies above the 'Caved' zone in these workings. The subsidence profile estimated by Saxena (2003) model was used to calibrate the properties of the 5 - 40 m thick 'Fractured' zone strata in these cases. The study revealed that the 'Ubiquitous-joint' material model with joint cohesion of 125 kPa and joint friction angle of 27° was able to replicate the maximum surface subsidence of 1.47-2.53 m corresponding to the extraction height of 2.2-3.7 m in these conditions. The initial modulus of the goaf material in these cases varied from 4.2-8 MPa. The model observed subsidence profile within the mining zone was closely reproduced by the empirical model. The subsidence profiles at the edges were also in line with the field observations reported by Singh and Yadav (1995) for the hard strata conditions.

Further study was made to evaluate the constitutive behaviour and model parameters of strata representing the 'Continuous Deformation' zone (CDZ) above the 'Fractured' zone. Four case

studies pertaining to panel 3 in Queen seam at JK5, panel 21 in coal seam 'I' of PVK 5, panel 4 in coal seam 'I' at VK7, and panel 1 in coal seam 'I' at ALP were considered at the cover depth of 188 – 465 m. The results of experimental modelling using the 'Ubiquitous-joint' material model established in Section 6.5, Chapter 6 was used to quantify the maximum extent of the Fractured zone and evaluate the reasonable properties of CDZ to reproduce the surface subsidence either observed in the field or estimated by the empirical model. Accordingly, the maximum extent of the Fractured zone was limited to 28 times the extraction height, and the strata within the CDZ were modelled as 'Transversely Isotropic Elastic' material with E_3/E_1 of 1.72 and G_{13} of 33 MPa. The results of all these models were validated in terms of the cover pressure distance (CPD) or the maximum pressure distance (MPD), maximum stress recovery, load transfer distance (LTD), and side abutment loading profile reported in the literature for similar conditions.

The side abutment stress followed an exponential decay profile with the distance from the panel edge in all the workings. These results were in line with the findings of Wilson (1983). The side abutment load in these works also agreed closely with the estimates of Mark (1987). The maximum stress recovery reached the cover pressure for supercritical longwall workings, while it was 54-79% of the cover pressure for subcritical workings. The CPD for supercritical workings ranged from 0.33-0.48 times, and the MPD for subcritical workings was 0.12-0.32 times the cover depth, which corroborated well with the findings of Smart and Haley (1987), Wilson (1981), King and Whittaker (1971), Choi and McCain (1980), Mark (1987), and Sheorey (1993). The peak side abutment stress varied between 2.26-3.42 times the in-situ vertical stress, which is in close agreement with the typical observations in the Indian coalfields, as reported by Singh and Singh (2009). However, the model observed load transfer distance (LTD) was 1.8-2.7 times greater than the simplified depth-dependent estimates of Peng and Chiang (1984), owing to the strong and massive nature of superincumbent strata in

the Indian geo-mining conditions. The other workers, such as Singh et al. (2011) and Larson (2015), also highlighted the influence of the strong and massive strata on the LTD.

Parametric Modelling Study

The Model I was used for evaluating the factor of safety and failure mechanism of the chain pillars for face length varying from 150-250 m, the cover depth from 350 to 900 m and different strength of the overlying strata and thicknesses of the strata in the Caved zone. The interfaces along the planes of contact at the roof-pillar and pillar-floor ends were assigned minimum normal and shear stiffness while ensuring compliance with the maximum permissible interface penetration as suggested in the manual. Their cohesion and friction angle values were assigned as 0.18 MPa and 27°, following the approach suggested in Das et al. (2019).

For evaluating the factor of safety of the chain pillar, the coal seam was modelled as ‘elastic’ material, while the rest of the strata were considered as ‘Mohr-Coulomb’ material at the virgin stage. The strata within the Caved zone were assigned the ‘Double-yield’ material model, while the ‘Fractured’ zone was assigned the ‘Ubiquitous joint’ model. In contrast, the CDZ was modelled as the ‘Transversely Isotropic elastic’ model. The floor strata were assigned Mohr-Coulomb strength properties considering competent strata formation of the sandstone, which is prevalent in most of the coalfields in India. Due care was taken in defining the abutment angle as per the findings of the study reported in Section 7.6, Chapter 7. Similar to the progressive mining practised in the field, the simulation of mining involved the development of gate roads considering the single or double row of chain pillars between the two adjoining panels. The size of the chain pillars for the single row configuration of the chain pillars varied from 25-100 m in the parametric study. A total of 1296 plain strain numerical models were studied to evaluate the FoS of the chain pillar in each condition.

The modelling results revealed that many of the input parameters were interrelated, although they seem independent in the preliminary stage. For example, the abutment angle was considered to be independent of the face length and depth of cover. However, the in-depth study indicated that it is affected by several factors. Under such conditions, the Machine learning (ML) tool was used to explain the complex interrelation between the control variables that affect the stability of the chain pillar in the ultimate stage of loading. This loading stage represented the condition when both the panels on either side of the chain pillar have been mined, and the chain pillar under consideration is beyond the zone of influence of the longwall faces. Thus, it considered the side abutment load being transferred on the pillars due to staged loading due to the sequential extraction of the panels and the damaged zones that form in the overlying strata in response to mining in the respective panels. A similar ML model was also worked out for the double row configuration of the chain pillars, wherein the size of the chain pillar varied from 10-47.5 m along with the same set of remaining input data.

The modelling results indicated that pillar width, coal strength, abutment angle, and modulus ratio of immediate roof and floor to the coal seam are positively correlated to the factor of safety of the chain pillars, while pillar height, cover depth, face length, caving height, overburden density and modulus of the strata in the CDZ are negatively correlated. Pillar width was the most influential parameter having a positive correlation with the stability of the chain pillar. At the same time, cover depth was the most critical parameter having an inverse relation with the stability of the pillar. The modulus ratio and strength of the immediate roof also played a significant role. The influence of face length, the density of roof layers and the modulus of the overburden strata had a marginal influence on the stability condition of the pillar.

The trends observed for the coal strength, pillar width, modulus ratio, cover depth, face length, and overburden density are broadly in line with the findings of Choi and McCain (1980), Hsuing and Peng (1985), Mark and Bieniawski (1986), and Colwell (1998). As noted by Frith

and Reed (2018), the increased spanning capability of the overburden strata over the caved goaf could lead to the increased load on the chain pillar, resulting in its reduced safety factor. The earlier works for the design of the chain pillar either considered a constant abutment angle or did not include its effect at all. Further, they estimated the strength of the pillar using an empirical formula and used the abutment angle only to determine the pillar load. These studies were not able to assess the influence of abutment angle on the pillar strength. The positive trend of the factor of safety of the chain pillar with abutment angle is due to increased pillar strength, resulting from improved confinement, which is in line with the observation of Chokhani (2012). The FoS of the chain pillar was negatively correlated to the caving height owing to an increase in the side abutment stress with the caving height (Rezaei et al., 2015c).

Case Studies

ALP Seam I Workings

The standard approach developed in this work was used to compare the pillar width practised in the field with the model estimated optimal size for six different mining locations at a cover depth varying from 392-865m and a face length of 95-250m. The abutment angle in these workings varied from 3-11°, as estimated using the statistical model developed in this work. In the elasto-plastic model, the coal seam was considered a strain-softening material with its post-failure parameters representing a large pillar. The strain-softening parameters for chain pillars were assigned according to their w/h ratio following the standard approach.

In ALP, the field size of the chain pillars between panels 1 and 2 of 250 m width at the cover depth of 465 m was 50 m, while the ML and the numerical model estimated optimal size was 51 m. The field size chain pillar between panels 2 and 3 at the cover depth of 519 was 63 m, while the ML model indicated optimum size was 58 m, and the numerical model estimated size was 56 m. Similarly, the field size chain pillar between panels 3 and 4 at the cover depth of

567 m was 69 m, while the ML model indicated optimum size was 61 m and the numerical model-based optimum pillar size was 60 m.

The in-depth stress analysis of side abutment loading and stress recovery in the goaf upon staged extraction of the adjoining panels in these working indicated that the peak side abutment stress varied from 1.9 to 2.04 times the in-situ vertical stress while the goaf stress recovery was 76-85% of the cover pressure upon extraction of the first panel. At the ultimate loading stage, the side abutment stress was 2.7-2.8 times the in-situ stress, while the stress recovery in the goaf reached 100% of the cover pressure for the pillar width of 50-69 m.

Although these pillars failed up to 9-12 m along their ribs, the weaker overlying strata suffered a significant failure. The stress recovery in the goaf achieved full cover pressure irrespective of the pillar size, as the roof strata could not sustain the highly concentrated stress due to lower strength, and the whole abutment load was ultimately transferred to the goaf. The plot of stress tensor adequately explained the role of confining stress on the stability of the chain pillars. Upon development of the gate road, the stress relaxed zone was formed only in a marginal portion along the ribs of the pillars, while the core of the pillar was only marginally concentrated of stress with respect to the virgin vertical stress. Upon mining of the first panel, the chain pillar developed a non-uniform side abutment load, and the confining stress also shifted accordingly to have further growth of the extent of the failure along the sides of the chain pillar. Upon mining of the second panel, the major principal stress continued to pass through the core of the pillar with readjustment of the confining stress, resulting in failure to the extent of 9-12 m on either side of the pillar. As the roof was comparatively weaker, it failed earlier before the pillar could crush. The abutment stress got redistributed upon failure in the roof. Thus, the integrity of the elastic core in the inter panel chain pillars of width as low as 50 m was still maintained.

The convergence and the lateral deformation of the pillar and coal ribs in the tailgate of the second panel varied between 83-106 mm, 53-78 mm and 17-31 mm respectively, in the three workings. The model observed tailgate convergence is in close agreement with the field observation. The modelling confirmed that it was possible to extract such workings with pillar size of 50 -60 m at the cover depth of 465 -567 m without any compromise on the safety of the mine workings.

Moonidih Colliery XVIII Seam Working

Upon mining of both the adjoining panels A4 and A5 of 95 m face length, the field size pillar of 45 m width in the 392 m deep XVIII seam at Moonidih Colliery experienced twin peaks of the side abutment stress with the maximum of 24 MPa, which is 3.2 times of the in-situ stress. The peak stress was realised at a distance of 12.5 m from the centre of the pillar. The maximum stress recovery in the goaf was 57-66 % in the adjoining panels. For the optimum width of 25 m, the goaf stress increased to 84-92%, while the side abutment stress in the pillar increased to 31.7 MPa, which is 4.1 times the in-situ vertical stress. This condition observed peak stress at the centre of the chain pillar. The field size pillar did not show any significant failure in the roof. However, failure reached the core of the optimum size pillar.

The confining stress and the extent of failure along the edges of the pillar showed a similar trend as observed in the ALP working, except that the failure in the relatively stronger roof was initiated after the failure in the coal pillar. The deformation in the gate road varied from 51 – 56 mm for the optimum pillar size. These deformation values agree with the field observations for acceptable performance of the chain pillar under given geo-mining conditions. A marginal increase in deformation with the reduction in pillar width from 45 m to 25 m implied that the latter could serve its design function without any compromise in the safety of the workings.

Moonidih Colliery XVI Top Seam Working

The field size pillar of 50 m between panels D12 and D13 in the XVI Top seam of Moonidih Colliery experienced twin peaks of the side abutment stress having a maximum of 52.7 MPa, which is 3.7 times the in-situ stress upon mining both the adjoining panels. The peak stress was observed at a distance of 14 m from the centre of the pillar. The maximum stress recovery in the goaf was 75 to 84% of the cover pressure in the adjoining panels. For the optimum pillar size of 34 m, although the goaf stress received only a marginal increase to 84 to 88%, the side abutment stress in the pillar increased to 67 MPa, which is 4.7 times the in-situ vertical stress. The peak stress was observed at a distance of only 4 m from the centre. The field size pillar did not show any significant failure in the roof. However, the failure reached the core along the contact surface of the roof and the pillar with a reduced pillar size corresponding to its optimum design. The confining stress and the extent of failure along the edges of the pillar showed a similar trend as observed in the previous case. However, the lateral deformation at the pillar and the coal ribs was significantly higher compared to the gate road convergence. A relatively marginal increase in the convergence and the lateral deformation with the reduced pillar size confirmed that the 34 m wide pillar could serve its design function without compromising the safety of the workings.

Moonidih Colliery XV Top Seam Working

The field size single row chain pillars of 60 m width between panels T3 and T4 in 865 m deep XV Top seam at Moonidih Colliery experienced peak abutment stress of 56.8 MPa, which is 3.8 times of in-situ vertical stress, while the failure extended to the core of the pillar during its ultimate stage of the loading. The stress recovery in the first panel was 88% of the cover pressure, while it was 80% in the second panel. Although the pillar failed up to its core, the roof was still stable. However, for the optimum pillar size of 52 m, the peak abutment increased

to 76.8 MPa, which is 4.5 times the in-situ stress, and the roof also received failure along with the failure of the pillar. The stress recovery in the first panel achieved the cover pressure, while it was 90% in the second panel. The lateral deformation and convergence in the gate road were significantly higher than the previous conditions owing to significantly higher cover depth. Such conditions demand a proactive supporting strategy to maintain the functional stability of the gate roads.

For double row configuration, the optimal size of the pillar between the panels T3 and T4 was 42 m compared to 52 m for the single row. The stress recovery in the goaf of the first panel was 100% of the cover pressure as observed in the previous case. However, in the second panel, it increased only marginally by 4% for the new configuration of the chain pillar. The chain pillar of reduced size received most of its failure upon mining the adjacent panel. However, its core and the remaining portion facing the middle gate road remained stable. Similar conditions developed for the second pillar upon mining the second panel. However, the gate road deformation increased significantly compared to the single-row pillars. It may be noted here that this model did not consider any support in the roof. Hence, the resultant deformation may be exaggerated compared to the supported excavation. Further, the stability of the pillars has been evaluated at its ultimate loading stage, representing a condition when both the panels have been excavated, and the pillar under consideration is beyond the zone of influence of the front abutment load of the individual panels. Moreover, the field experience in similar conditions in other countries has established that it is possible to maintain acceptable roof conditions in such workings by taking care of the yield zone in the roof and sides of the gate roads. Under these conditions, it is expected that the optimum size pillar of 42 m with the double row configuration would serve its design function of serviceable gate roads and efficient ventilation to the highly gassy workings at such a high depth of cover of the chain pillars.

The cover pressure distance (CPD) in the modelled cases varied from 0.06 - 0.12 times the cover depth. The observed CPD was lower as compared to the previous findings of Smart and Haley (1987), Wilson (1981), King and Whittaker (1971), Choi and McCain (1980), Mark (1987), and Sheorey (1993). It was mainly because of the different considerations to the abutment angle, which ranged from 3-11° depending upon the geo-mining conditions. In comparison, the previous workers assumed a relatively higher abutment angle of 18, 21, and 31°.

Conclusions

The following conclusions can be drawn based on the study conducted in this dissertation:

- i. A numerical modelling approach has been developed to design optimal size chain pillars for deep longwall workings in Indian geo-mining conditions. It considered a calibrated 'Double-yield' material model for simulating stress recovery in goaf material, 'Ubiquitous joint' model for simulating damage in the 'Fractured' zone, and 'Transversely Isotropic Elastic' model for the 'Continuous Deformation' zone (CDZ). The estimation of abutment angle and the post-failure strain-softening behaviour of different w/h ratios of the chain pillars were also explained through empirical relations.
- ii. The abutment angle was not constant across the geo-mining condition of the longwall working. It was negatively correlated with the cover depth and the face length and positively correlated with the strata strength. It also depended on the thickness ratio of the strata within the Caved zone and the face length. Cover depth was the most critical parameter.
- iii. The post-failure degradation of the cohesion was positively correlated with the uniaxial compressive strength, w/h ratio, elastic modulus, and the zone size and

negatively correlated with the friction angle. The residual value of cohesion was positively correlated with the w/h ratio.

- iv. The degradation rate of friction angle was constant, while its residual value was positively correlated with the w/h ratio and negatively correlated with the peak friction angle.
- v. The interface along the planes of contact of the roof – pillar and floor – pillar and the zone size of the pillar had a significant influence on the post-failure behaviour of the pillar.
- vi. Pillars having a w/h ratio less than 2 showed a brittle failure, while those with a w/h ratio of 2-6 showed a strain-softening behaviour. Pillars with a w/h ratio of more than 6 showed a positive volumetric strain trend in response to the axial strain during the uniaxial loading, confirming its strain hardening behaviour.
- vii. The standard approach for simulating the loading behaviour and study of the factor of safety led to the development of a machine learning (ML) based model for the rational design of the chain pillars. The FoS-based design criterion for chain pillars was developed by simulating the failed and stable cases of 43 support pillars in different coal seams in India. The median FoS of 0.78 of the failed pillars represented the optimum size pillars.
- viii. For Adriyala Longwall Project workings, the pillars implemented in the field were 12.5-15% wider as compared to the optimum size as estimated in this study.
- ix. The pillar width of 25 m proved to be optimum in place of the field size pillar of 45 m for working 95 m wide longwall panels A4-A5 in 392 m deep coal seam XVIII at Moonidih Colliery. The rational size of chain pillar between panels D12 and D13 of 150 m face length in XVI seam working at this mine at a cover depth of 580 m was estimated as 34m compared to 50 m as implemented in the field.

- x. The 60 m wide chain pillars in the single row layout between the panels T3 and T4 of 250 m face length in XV Top coal seam at Moonidih Colliery proved to be oversized by 15% compared to the optimum size of 52 m at the cover depth of 865 m at Moonidih Colliery. For double row configuration, the optimal size of pillars was further reduced to 42 m.
- xi. The oversized pillars either showed incomplete failure even after the extraction of both the adjoining panels or lesser stress transfer in the goaf area at the cost of wastage of mineral undesirably locked up in the chain pillars. The optimum size pillars not only ensured its controlled settlement during sequential mining of the adjoining panels but also helped in a reasonable stress transfer in the caved goaf that had a more significant role in defining the overall ground control after the extraction of the panels.
- xii. The lateral deformation in the gate road and the edges of the chain pillars increased with the increasing cover depth and reduced pillar width. A proactive supporting strategy was required to effectively control plastic deformation and the sustainable serviceability of gate roads in such conditions.
- xiii. The concentration of side abutment load for weaker immediate roof conditions led to its failure before the coal pillar could undergo failure, thus, limiting the role of the pillar on the overall stability in such workings.
- xiv. The machine learning model for the single and double row configurations of the chain pillars revealed that the factor of safety of the chain pillar is positively correlated with the pillar width, coal strength, abutment angle, and the ratio between the modulus of the coal seam and the roof and floor strata. It showed a negative correlation with the pillar height, cover depth, face length, caving height, unit weight and modulus of the overburden strata.

- xv. Except ALP working, the oversized pillars in rest of the cases had an intact core of 24 to 28 m even after extraction of both the adjoining panels compared to approximately no intact zone in the optimal size pillars. In the case of ALP working, the failure in the pillar system was governed by the behaviour of the weak immediate roof.
- xvi. The maximum side abutment load varied between 1.78 to 2.83 times the in-situ vertical stress for cover depth varying from 392 to 865 m and face length varying from 95 to 250 m.
- xvii. The caved goaf achieved the cover pressure in most of the subcritical deep longwall workings with the optimal size of the intervening chain pillars.
- xviii. The distance to the maximum stress recovery in the goaf was $0.06 - 0.12H$ compared to $0.12 - 0.6H$ reported earlier.

CONTENTS

CHAPTER	TITLE	PAGE
	Certificate	II
	Declaration by the Candidate	III
	Copyright Transfer Certificate	IV
	Acknowledgement	V
	Abstract	VI
	Contents	XXVI
	List of Tables	XXXI
	List of Figures	XXXV
	Notations, Symbols and Abbreviations	XLIII
1.	Introduction	1-8
	1.1 Objective and scope	5
	1.2 Methodology	6
	1.3 Organization of the thesis	7
2.	Literature Review	9-59
	2.1 General	9
	2.2 Mechanics of Rock Damage and Stress Redistribution	9
	2.3 Progressive Loading of Chain Pillars	19
	2.4 Strength of the Pillar	29
	2.5 Global Experience of the Chain Pillar Design	32
	2.6 Important Considerations in the Chain Pillar Design	40
	2.6.1 Safety Factor of Chain Pillar	40
	2.6.2 Stress-Strain Behaviour of Rocks	42
	2.6.3 Effect of Interface Friction, w/h and W/L Ratios	46
	2.6.4 Constitutive Behavior of the Caved Goaf	55
	2.7 Summary	56

3.	Research Methodology and Numerical Model Formulation	60-91
3.1	General	60
3.2	Model Formulation	61
3.3	Assessment of Roof Layers and their Mechanical Properties	63
3.4	Simulation of Parting Planes	64
3.5	Constitutive Model	67
	3.5.1. Selection of Material Model for Rock Mass	71
	3.5.2. Post-failure Degradation of Strength Parameters	72
3.6	Estimation of the Rock Mass Properties	73
3.7	In-situ Stress Field	76
3.8	Two-dimensional Model for Chain Pillar Stability (Model I)	77
3.9	Estimation of Rock Mass Parameters for Fractured and Continuous Deformation zones (Model VI)	79
3.10	Derivation of the Strain Softening Parameters (Model III)	80
3.11	Study of Failed and Stable Pillars (Model IV)	83
3.12	Study of Goaf Behaviour Control Parameters (Model II)	85
3.13	Assessment of Abutment Angle in Longwall Workings (Model V)	86
3.14	Design Criterion For Chain Pillars	89
3.15	Summary	90
4.	Numerical Simulation of the Strain-Softening Behaviour	92-116
4.1	General	92
4.2	Constitutive Behaviour	92
4.3	Post-peak Strength Parameters	95
4.4	Drop Rates and Residual Cohesion and Friction angle	97
4.5	Statistical Models for Post-Peak Strength Parameters	108
4.6	Model Validation	110
4.7	Summary	115

5.	Criterion for Factor of Safety of Chain Pillar	117-131
5.1	General	117
5.2	Failed and Stable Pillar Cases	117
5.3	Estimation of Rock Mass Properties of Coal	119
5.4	Numerical Modeling of the Pillar	121
5.5	Modeling Results	122
5.6	Design Criterion	130
5.7	Summary	130
6.	Strength and Deformability Parameters of the Damaged Zones	132-159
6.1	General	132
6.2	Delimitation of the Zones in the Area of the Excavation	133
6.3	Selection of Material Models	135
6.4	Model Parameters for the Caved Goaf Material	136
6.5	Fractured zone Model Parameters	141
6.6	Model Parameters for the Continuous Deformation zone	146
6.7	Verification of Modelling Results	153
6.8	Summary	157
7.	Determining Abutment Angle for Varying Geo-Mining Conditions	160-173
7.1	General	160
7.2	Mechanism of Formation of the Abutment Angle	160
7.3	Identification of Parameters affecting Abutment Angle	162
7.4	Numerical Modelling Study	163
7.5	Model Observations	165
7.6	Statistical Model for Estimation of the Abutment angle	169
7.7	Model Verification	171
7.8	Summary	172

8.	Study of the Chain Pillars Stability in Longwall Workings	174-188
8.1	General	174
8.2	Development of Predictive Model for Factor of Safety	178
	8.2.1. Model for Single Row Configuration of Chain Pillars	182
	8.2.2. Model for Double Row Configuration of Chain Pillars	183
8.3	Performance Evaluation of the Model	184
8.4	Influence of Critical Parameters on the Stability of Chain Pillars	185
8.5	Summary	188
9.	Case Studies for the Optimum Design of Chain Pillars in Deep Longwall Workings	189-253
9.1	General	189
9.2	Site and Geo-mining Details	190
	9.2.1 Adriyala Longwall Project	190
	9.2.2 Moonidih Colliery	193
	9.2.2.1 The XVIII Seam working	194
	9.2.2.2 The XVI Top Seam Working	196
	9.2.2.3 The XV Seam Working	198
9.3	Determination of the Optimum Pillar Size	199
9.4	Elasto-Plastic Modelling Results	204
	9.4.1. Chain pillar between Panels P1-P2 in Adriyala Seam-I Working	205
	9.4.2. P2-P3 Chain pillar in Adriyala Seam-I Working	213
	9.4.3. Chain Pillar between panels P3-P4 in Adriyala Seam-I Working	216
	9.4.4. Chain Pillars Between Panels A4-A5 in Moonidih XVIII Seam Working	218
	9.4.5. Chain Pillars between Panels D12-D13	224
	9.4.6. Single Row Pillar between Panels T3- T4 in XV Top Seam Working at Moonidih Colliery	229
	9.4.7. Double Row Pillar between Panels T3- T4 in XV Top Seam Working at Moonidih Colliery	236

9.5	Summary	244
10.	Discussion and Conclusion	254-273
10.1	Discussion	254
10.2	Conclusion	270
10.3	Future Scope of Work	273
	REFERENCES	274
	ANNEXURE I	287
	ANNEXURE II	293
	ANNEXURE III	296
	ANNEXURE IV	299
	ANNEXURE V	301
	ANNEXURE VI	304
	ANNEXURE VII	371

LIST OF TABLES

TABLE	TITLE	PAGE
CHAPTER 2		
2.1	Abutment angle observed by various researchers	28
2.2	Pillar strength formulae developed by different authors	29
2.3	Suggested stability factor for different competency of roof (Cowell, 1998)	41
2.4	Post-peak strength parameters of the coal used by previous researchers	44
CHAPTER 3		
3.1	Constitutive models for different rock behaviour	67
3.2	Parameters of the W-D dilation angle model (Walton and Diederichs, 2015)	73
CHAPTER 4		
4.1	Interface properties considered in the model	97
4.2	Input parameters of the W-D dilation angle model used in the numerical modelling (after Walton and Diederichs, 2015)	97
CHAPTER 5		
5.1	Collated data of failed pillar cases	118
5.2	Collated data of stable pillar cases	119
5.3	Pillar load and strength of failed pillars along with their factor of safety	122
5.4	Pillar load and strength of stable pillars along with their factor of safety	123
CHAPTER 6		
6.1	Typical material properties of the Double yield model	140
6.2	The geo-mining details of the supercritical longwall panels	141
6.3	Characteristics of the roof strata and their geotechnical properties in the supercritical workings	142
6.4	Rock mass input properties of Workings ‘A’, ‘B’, ‘C’, and ‘D’	143

6.5	The geo-mining details of the subcritical longwall panels	147
6.6	The characteristics of the roof strata and their associated geotechnical properties in the considered subcritical workings.	147
6.7	Rock mass properties of Workings ‘P’, ‘Q’, ‘R’, and ‘S’	148
CHAPTER 7		
7.1	Statistical summary of the considered parameters in the model	170
7.2	Comparison of the model estimated abutment angle with the findings of Das (2000) in Indian longwall workings	172
CHAPTER 8		
8.1	Geo-mining details of the longwall panels	174
8.2	R^2 , RMSE, VAF, and MAPE of the SVR model for training and testing data sets of single and double row chain pillars	185
8.3	Basic value of the critical parameters and their range of variation and interval for single and double row chain pillars	185
CHAPTER 9		
9.1	The geo-mining details of the case studies	189
9.2	The characteristics of the roof strata and their properties in Panel P1	192
9.3	Rock characteristics of the strata overlying A4 panel at Moonidih mine	195
9.4	Physico-mechanical properties of strata in XVI Top seam Working at Moonidih Colliery	197
9.5	Physico-mechanical properties of XV Top and Botoom Coal Seams and its Parting at Moonidih mine	199
9.6	Rock mass properties for the numerical model of Longwall Workings at Adriyala Longwall Project and Moonidih Colliery	200
9.7	Material properties of the Double yield model for Caved Goaf	201
9.8	Material properties of the Transversely Isotropic model and the Abutment angle	201
9.9	Safety factor of chain pillars implemented in the field and their optimum width	204

9.10	Geo-mining and strength parameters of the pillars and their optimum size for single-row configuration	246
9.11	Model Observed convergence and the ribs closure in the tail gate of the second panel after extraction of the first panel	251
9.12	The peak abutment stress and the goaf stress recovery in the workings under study with optimum pillar width	252

ANNEXURE I

AI.1	Properties of rock beds lying above W2 panel in RVII coal seam at Jhanjra mine ECL	287
AI.2	Properties of rock beds lying above panel 1 in Passang seam at Balrampur mine SECL	287
AI.3	Properties of rock beds lying above panel K5 in Passang seam at New Kumda mine SECL	287
AI.4	Properties of rock beds lying above P2 panel in Burhar VIB seam at Rajendra mine SECL	288
AI.5	Properties of rock beds lying above panel 3 in Queen seam at JK 5 mine SCCL	288
AI.6	Properties of rock beds lying above panel 21 in Top seam at PVK mine SCCL	288
AI.7	Properties of rock beds lying above panel 4 in Top seam at VK 7 mine SCCL	289
AI.8	Properties of rock beds lying above panel 1 in No. I seam at Adriyala mine SCCL	289
AI.9	Properties of rock beds lying above A4 panel in XVIII coal seam at Moonidih mine BCCL	290
AI.10	Properties of rock beds lying above panel D13 in XVI Top seam at Moonidih mine BCCL	290
AI.11	Properties of rock beds lying above panel T3 in XV Top seam at Moonidih mine BCCL	291

ANNEXURE II

AII.1	Rating of RSI Parameters	294
-------	--------------------------	-----

ANNEXURE III

AIII.1	The final values of cohesion and friction angle drop rates and their residual values of coal samples of different w/h ratios from six Indian seams	296
--------	--	-----

ANNEXURE IV

AIV.1	Parametric modelling results of the three-dimensional models for determining the abutment angle	299
-------	---	-----

ANNEXURE VI

AVI.1	Parametric modelling results of the plain-strain models for determining the factor of safety of the single row chain pillar	304
AVI.2	Parametric modelling results of the plain-strain models for determining the factor of safety of the double row chain pillar	333

LIST OF FIGURES

TABLE	TITLE	PAGE
CHAPTER 2		
2.1	Damage zones above a longwall face	10
2.2	Probable strata condition in the vicinity of a longwall face with a weak immediate roof	11
2.3	Redistribution of strata pressure at the seam level around the goaf area	12
2.4	Distribution of the vertical stress in the coal seam	14
2.5	Main roof failure for different ratios of the lateral dimensions	15
2.6	Subsidence observed in Indian coal mines	18
2.7	Schematic diagram depicting various stages of loading of a chain pillar	20
2.8	(i) Maximum width of pressure arches observed in British mines and (ii) schematic diagram of load deficiency in the goaf	23
2.9	The estimation of the load on the chain pillar using the concept of shear angle	25
2.10	Overburden displacement zone above a mined-out longwall panel	26
2.11	Determination of chain pillar width using the load balance scheme	38
2.12	Plan showing disturbed zone in the roadway of a longwall panel in Moonidih	39
2.13	Stress-strain curves of the sandstone triaxial tests	42
2.14	Influence of w/h ratio on the post-failure behaviour of the coal samples	43
2.15	Influence of low shear strength contact surface on the mode of failure of the specimen	47
2.16	Stress-strain characteristics and failure behaviour of an in-situ pillar of 2m width and 1m height at different stages of loading	48
2.17	The three zones in the yield pillar based on the level of confinement	49
2.18	The evolution of minimum principal stresses with various w/h ratios and interface properties	50
2.19	The four zones identified on the top end surface of a coal sample of w/h=12	51

2.20	The input parameters of the parallelogram-shaped pillar	53
2.21	Variation of pillar strength with the length to width ratio (l/w) and width to height ratio (w/h)	54

CHAPTER 3

3.1	Flow chart showing the linkage between various numerical models, the outcomes of the model at the tail of the arrow line were utilised as the input for the model at the head	62
3.2	Generic layout of a longwall working showing the plane of consideration XZ in Model I	63
3.3	Schematic diagram depicting the component of the constitutive model of an interface node	65
3.4	Consideration of zone dimension for interface stiffness	66
3.5	Mohr-Coulomb failure criterion with tension cut-off	70
3.6	The geometry and boundary conditions of the plain-strain model	78
3.7	The geometry and boundary conditions of the plain-strain model employed to determine the rock mass parameters	80
3.8	Geometry of coal sample models of different diameter to height ratio	82
3.9	Boundary condition for coal sample of $w/h=1.0$	83
3.10	Geometry of the pillar model along with its boundary conditions	84
3.11	(a) Load deformation set up for confined uniaxial testing of graded down goaf material; (b) simulated goaf material after completion of the test; and (c) numerical model for replicating the laboratory tests	86
3.12	Geometric view of the three-dimensional model	88

CHAPTER 4

4.1	Effective friction angle of the surface due to surface roughness and normal stress	94
4.2	Charts depicting the input properties of coal in the model	96
4.3	Schematic illustrating the evolution of strength components, friction angle and cohesion as a function of inelastic strain in the MCSS constitutive model	98
4.4	The scheme of the iterative technique used to calibrate the model stress-strain curve against the laboratory curve for a give w/h ratio sample based on hit-and-trial	99

4.5	Comparison between the model observed and the laboratory test results of the coal samples of varying w/h ratio from the Singhpur middle seam	101
4.6	Volumetric-axial strain curves of the Singhpur middle coal sample models of various w/h ratio	102
4.7	Mobilised dilation angle vs plastic shear strain curves of Singhpur middle coal sample models of various w/h ratio	103
4.8	Stress-strain profiles of axial and confining stresses for Singhpur middle coal samples of w/h ratio of 0.5, 4.5, 7.7, and 13.5, depicting different post-failure behaviour: brittle, softening, ductile, and continuous strain-hardening	104
4.9	Slip along the interface due to shearing, failure state of the top end-surface of the coal sample, and shear displacement of the interface for samples having w/h ratio of (a) 0.5, (b) 4.5, (c) 7.7, and (d) 13.5 at the loading stage highlighted by the cross, circle, triangle, and rhombus markers as shown in Figure 4.8	106
4.10	Model observed volumetric strain vs differential stress, illustrating relative volumetric changes due to new cracks formation or propagation of existing ones and compaction of pores or existing cracks	107
4.11	Comparison between the statistically predicted values and the numerical model for (a) cohesion drop rate (b) residual cohesion and (c) residual friction on a logarithmic scale	109
4.12	Drop rate, peak, and residual values of (i) cohesion and (ii) friction angle of the coal samples of (a) 61 and (b) 146 mm diameter	111
4.13	The comparative plot of the laboratory tests results and numerical model of (i) axial stress – strain and (ii) volumetric – axial strain for confining stress of (a) 0.2, (b) 2.0, and (c) 5.0 MPa for 61 mm diameter coal samples	112
4.14	Laboratory tests results vs the numerical model results of axial stress – strain (a) and volumetric - axial strain (b) at confining stress of 0.2, 1.0, 2.0, and 3.0 MPa for 146 mm diameter coal samples	113
4.15	Failure mechanism observed in the laboratory tests (top) and numerical models (bottom) for confining stresses of (a) 0.2, (b) 2.0, and (c) 5.0 MPa	114

CHAPTER 5

5.1	Estimated values of RMR76 for all pillar cases	121
5.2	Model strength versus pillar load of the failed and stable pillar cases from Table 5.3 and 5.4	124
5.3	Factor of safety of the failed and stable pillars, the horizontal line at the safety factor of '1' separates most of the failed and stable pillars quite successfully	125
5.4	Stress – strain behaviour of pillars for the failed cases 2 and 21 and the stable case 10	126

5.5	Pattern of (a) failure, (b) Vertical stress, (c) interface shear slip and displacement at upper and lower halves of the pillar at (p) two-third of peak strength, (q) peak strength, and (r) residual strength of stable pillar case 10.	128
-----	--	-----

CHAPTER 6

6.1	The damaged strata above a longwall panel due to extraction of the underlying seam	134
6.2	Comparison of the calibrated numerical model results with Salamon (1990) model for varying initial modulus and bulking factor	140
6.3	Bar chart illustrating the values of initial gob modulus in the four supercritical workings	145
6.4	Comparison of model subsidence results with the empirical subsidence model	145
6.5	Geological Strength Index chart	150
6.6	Bar chart illustrating the values of initial gob modulus in the four subcritical workings	152
6.7	Comparison of modelled subsidence results with the empirical subsidence model and in the case of Working 'S' with field measured subsidence	152
6.8	Distribution of vertical stress at the seam level at the pre-mining stage (black dotted line), post-mining stage (solid green line), and Wilson's (1983) abutment stress decay curve fitted to the model abutment stress profile (solid yellow line) for (a) Working 'A' and (b) Working 'P'	154
6.9	Bar charts illustrating (a) the side abutment load and its comparison with Mark (1987), (b) maximum pressure distance (MPD), (c) peak side abutment stress and maximum recovered gob stress, and (d) load transfer distance (LTD) and its comparison with Peng and Chiang (1984) in the supercritical and subcritical workings	156

CHAPTER 7

7.1	Formation of abutment along the panel edge in a typical longwall working	161
7.2	Variation of (i) cover depth and (ii) thickness ratio for estimation of the abutment angle	164
7.3	Three-dimensional view of the measured abutment angle in case of experimental models with (a) soft strata and (b) hard strata conditions at the cover depth of 600m with face length of 200 m and thickness ratio of 2	166
7.4	Variation of the model observed abutment angle with (a) the cover depth and strata condition, (b) the cover depth and face length, and (c) the cover depth and thickness ratio	168

CHAPTER 8

8.1	Parametric study variables and their range	177
8.2	Defined hyperplane with an ε tolerance of error and slack variables	179
8.3	Cross-validation of SVR model for single-row chain pillars; comparison of the predicted and the actual factor of safety values for (a) training set and (b) testing set	182
8.4	Variation of residual error values as predicted by SVR model for the single-row configuration of chain pillars	183
8.5	Cross-validation of SVR model for double row chain pillars; comparison of the predicted and actual factor of safety values for (a) training set and (b) testing set	183
8.6	Variation of residual error as predicted by SVR model for the double-row configuration of chain pillars	184
8.7	Variation in the factor of safety of the single and double-row chain pillars with the parametric study variables	187

CHAPTER 9

9.1	Geological map of Godavari Valley Coalfield and location of the Adriyala longwall project	191
9.2	Layout of the mine plan of the Adriyala Longwall Project	192
9.3	Cumulative convergence in the tailgate with time and the retreat of the face in the first panel	193
9.4	Geological map of Jharia Coalfield and location of the Moonidih mine	194
9.5	Part plan showing the location of longwall panels in XVI Top seam	197
9.6	Part plan showing the location of proposed longwall panels in XV Top and Bottom coal seams	198
9.7	Variation in the factor of safety of the chain pillars of different widths between (i) P1-P2, (ii) P2-P3, (iii) P3-P4, (iv) A4-A5, (v) D12-D13, (via) T3-T4 Single row, and (vib) T3-T4 Double row	203
9.8	Distribution of vertical stress in the chain pillars of (a) 50, (b) 60 (c) 70 and (d) 80 m width	206

9.9	Terminology used to locate the study point and describe the distribution of vertical stress and failure in the chain pillar	207
9.10	Block contour of vertical stress distribution with one-sided and both-sided goaves for pillar widths of (a) 50, (b) 60, (d) 70, and (d) 80 m	209
9.11	Failure in the chain pillar with one-sided and both-sided goaves for pillar width of (a) 50, (b) 60, (d) 70, and (d) 80 m	210
9.12	Principal stress tensor plot showing confining stress for pillar width of 50 m at different loading stages	212
9.13	Model observed convergence in the tailgate and lateral deformation in the coal and pillar ribs of the second panel for pillar widths of 50, 60, 70, and 80m	213
9.14	Distribution of vertical stress in the chain pillars of (a) 56 and (b) 63 m width	214
9.15	Model observed convergence in the tailgate and lateral deformation in the coal and pillar ribs of the second panel for chain pillar widths of 56 and 63 m	215
9.16	Distribution of vertical stress in the chain pillars of (a) 60 and (b) 69 m width	216
9.17	Model observed convergence and lateral deformation in the coal and pillar ribs in the tailgate of the second panel for chain pillar widths of 60 and 69 m	217
9.18	Distribution of vertical stress in the chain pillars of (a) 25, (b) 35 and (c) 45 m width	219
9.19	Failure state of the pillar system with one-sided goaf and both-sided goaf for pillar widths of (a) 25, (b) 35, and (c) 45 m	220
9.20	Block contour of vertical stress distribution with one-sided goaf and both-sided goaf for pillar widths of (a) 25, (b) 35 and (b) 45 m	222
9.21	Principal stress tensor plot showing confining stress for pillar width of 25 m at different loading stages	223
9.22	Convergence and lateral deformation in the coal and pillar ribs in the tailgate of the second panel for pillars of 25, 35, and 45 m width	224
9.23	Distribution of vertical stress in the chain pillars of (a) 34 and (b) 50 m width	225
9.24	Failure state of the pillar system with one-sided goaf and both-sided goaf for pillar widths of (a) 34 and (b) 50 m	226

9.25	Block contour of vertical stress distribution with one-sided goaf and both-sided goaf for pillar widths of (a) 34 and (b) 50 m	227
9.26	Principal stress tensor plot showing confining stress for pillar width of 34 m at different loading stages	228
9.27	Gate road convergence and lateral deformation in coal and pillar ribs of the second panel for pillar widths of 34 and 50 m	229
9.28	Distribution of vertical stress in the chain pillars of (a) 52, (b) 60, and (a) 70 m width	230
9.29	Failure state of the pillar system with one-sided goaf and both-sided goaf for pillar widths of (a) 52, (b) 60, and (c) 70 m	232
9.30	Block contour of vertical stress distribution with one-sided goaf and both-sided goaf for pillar widths of (a) 52, (a) 60, and (c) 70 m	234
9.31	Principal stress tensor plot showing confining stress for pillar width of 52 m at different loading stages	235
9.32	The convergence and lateral deformation in the coal and pillar ribs in the tailgate of the second panel for pillar widths of 52, 60, and 70 m.	236
9.33	Intervening chain pillars and the longwall panels along with the study point in the chain pillar to explain the distribution of vertical stress and failure	237
9.34	Distribution of vertical stress in the chain pillars of (a) 42 and (b) 52 m width	238
9.35	Failure state of the pillar system with one-sided goaf and both-sided goaf for pillar width of (a) 42 and (b) 52 m	239
9.36	Block contour of vertical stress distribution with one-sided goaf and both-sided goaf for pillar widths of (a) 42 and (c) 52 m	240
9.37	Principal stress tensor plot showing confining stress for pillar width of 42 m at different loading stages	242
9.38	Tailgate convergence and lateral deformation in entries 1 and 2 of the second panel for pillar widths of 38, 42, and 52 m upon extraction of the first panel	243
9.39	Typical support system for containing deformation in longwall gate roads	244

ANNEXURE V

AV.1	Distribution of vertical stress at the seam level at the pre-mining stage, post-mining stage, and Wilson's (1983) abutment stress decay curve fitted to the model abutment stress profile for Working 'B'	301
AV.2	Distribution of vertical stress at the seam level at the pre-mining stage, post-mining stage, and Wilson's (1983) abutment stress decay curve fitted to the model abutment stress profile for Working 'C'	301
AV.3	Distribution of vertical stress at the seam level at the pre-mining stage, post-mining stage, and Wilson's (1983) abutment stress decay curve fitted to the model abutment stress profile for Working 'D'	302
AV.4	Distribution of vertical stress at the seam level at the pre-mining stage, post-mining stage, and Wilson's (1983) abutment stress decay curve fitted to the model abutment stress profile for Working 'Q'	302
AV.5	Distribution of vertical stress at the seam level at the pre-mining stage, post-mining stage, and Wilson's (1983) abutment stress decay curve fitted to the model abutment stress profile for Working 'R'	303
AV.6	Distribution of vertical stress at the seam level at the pre-mining stage, post-mining stage, and Wilson's (1983) abutment stress decay curve fitted to the model abutment stress profile for Working 'S'	303

Notations, Symbols and Abbreviations

a	A dimensionless constant
A_b	Stress in the yielded zone of the pillar
A_p	Cross-section area of the pillar
A_w	Stress deficiency in the goaf area
b	Bulking factor of the gob material
b_i	Represents the exponent of the failure criterion for intact rock
b_m	Represents the exponent of the failure criterion for rock mass
B	Bord width
c	Cohesion
c_{drop}	Drop rate for cohesion
c_j	Joint cohesion
c_{peak}	Peak value of the cohesion
c_{res}	Residual value of the cohesion
C	Constant associated with the zone of influence
C_p	Circumference of the pillar
d	Diameter of the specimen
dd	Dip direction of the plane of isotropy
dip	Dip angle of the plane of isotropy
D	Degree of disturbance
e_1	Young's modulus of the plane of isotropy
e_3	Young's modulus in the plane normal to the plane of isotropy
e^{ps}	Plastic shear strain
e^{pt}	Plastic tensile strain
e^{pv}	Plastic volumetric strain
e_c^{ps}	Plastic shear strain corresponding residual cohesion value
e_ϕ^{ps}	Plastic shear strain corresponding residual friction angle
E	Elastic modulus
E_0	Initial tangent modulus
E_c	Elastic Modulus of Coal
E_f	Elastic Modulus of Floor
E_i	Elastic Modulus of Immediate Roof

E_m	Elastic Modulus of Main Roof
f^s	Shear yield function
f^t	Tension yield function
f^v	Volumetric yield function
F	Front abutment factor
F_L	Face length
g13	Shear modulus normal to the plane of isotropy
g^s	Shear plastic potential function
g^t	Tension plastic potential function
g^v	Volumetric plastic potential function
G	Shear modulus
G_T	The average value of geothermal gradient
h	Pillar height
h_c	Height of the Caved zone
h_e	Height of the extraction
h_f	Height of the Fractured zone
H	Depth of Cover
k_c	Strength of 25mm (1 inch) cubic coal sample
k	Strength of 0.3m (1 ft) cubical coal sample (critical size)
K	Bulk modulus
$K(x_i, x_j)$	Kernel function
l	Pillar length
L	Longwall panel length
L_D	Development Load Per Unit Length of the Pillar
L_f	Front Abutment Load per Unit Length of Gate Entry
L_s	Side Abutment Load per unit length of gate entry for critical and supercritical panels
L_{ss}	Side Abutment Load per unit length of gate entry for subcritical panels
nu12	Poisson's ratio in the plane of isotropy
nu13	Poisson's ratio in the plane normal to the plane of isotropy
p	A constant for broken coal
p_c	Cap pressure
P	Width of the panel

q	Triaxial constant
R	Multiplication factor
R_0	Critical w/h ratio of the pillar
R_l	Lower limit of R_P
R_P	w/h ratio of the pillar
R_u	Upper limit of R_P
S	Pillar strength
S_{3c}	Triaxial strength
S_c	Compressive strength of the coal specimen
t	Thickness of rock bed
T_{IR}	Thickness of the immediate roof
T_{MR}	Thickness of the main roof
V	Pillar volume
w	Pillar width
w_e	Roadway width
w_{ep}	Effective width of the pillar
\bar{x}	Width of the yield zone in the pillar
z_s	Zone size
α_0	Determines the curvature of the pre-mobilization portion of the curve for $\sigma_3 = 0$
α'	Determines how the pre-mobilisation curvature changes as a function of σ_3
β	Abutment angle (or Shear Angle or Negative Angle of Draw)
β_T	Coefficient of thermal expansion
γ	Average unit weight
γ^p	Current value of the plastic shear strain
γ'	Defines the decay rate of the dilation angle post-mobilisation for non-zero confinement
γ_0	The decay rate of the dilation angle post-mobilisation for zero confinement
γ_m	Plastic shear strain at which peak dilation is achieved
γ_{IR}	Effective unit weight of the immediate roof
γ_{MR}	Effective unit weight of the main roof
δ_{ij}	Kronecker delta symbol
Δz_{min}	The smallest width of the neighbouring zone in the normal direction

ε	Axial strain
ε_m	Maximum possible compressive strain
ε_p	A constant in Salamon and Wagner (1985) formula
λ	A dimensionless constant
μ_{0m}	Coefficient of the internal friction angle
ν	Poisson's ratio
ξ_i	Positive slack variables
$\rho_{imm.}^{avg.}$	Thickness weighted average of the density of the immediate roof rocks
σ	Stress
σ_1	Major principal stress
σ_2	Intermediate principal stress
σ_3	Minor principal stress or confining stress
σ_c	Compressive strength of the intact rock
σ_{cm}	Compressive strength of the rock mass
σ_h	Average horizontal stress
σ^t	Tensile strength
σ_j^t	Joint tension limit
σ_m	Equivalent tensile strength
σ_{mIR}	Equivalent tensile strength of the immediate roof
σ_{mMR}	Equivalent tensile strength of the main roof
σ_t	Tensile strength of the intact rock
σ_{tm}	Tensile strength of the rock mass
σ_v	Vertical stress
τ_{sm}	Shear strength
ϕ	Dilation angle
ϕ_{drop}	Drop rates of the friction angle
ϕ_i	Initial value of the friction angle
ϕ_j	Joint friction
$\phi_{res.}$	Residual value of the friction angle
$\phi(x)$	Non-linear mapping function

Abbreviations

CPD	Cover Pressure Distance
DISL	Damage Initiation Spalling Limit
CMR	Coal Mine Regulations
FLAC	Fast Lagrangian Analysis of Continua
DGMS	Directorate General Of Mines Safety
MPR	Maximum Pressure Recovery
MPD	Maximum Pressure Distance
FoS	Factor of Safety
LTD	Load Transfer Distance
NEW	Non-Effective Width to Depth Ratio of the Panel
ALPS	Analysis of Longwall Pillar Stability
ALTS	Analysis of Longwall Tailgate Serviceability
CMRR	Coal Mine Roof Rating
HDZ	Height of Distressed Zone
RSI	Roof Separation Index
RQD	Rock Quality Designation
UCS	Uniaxial Compressive Strength
MC	Mohr-Coulomb
MCSS	Mohr-Coulomb Strain Softening
GSI	Geological Strength Index
NURBS	Non-Uniform Rational Basis Spline
GRC	Ground Response Curve
TAT	Tributary Area Theory
RMR	Rock Mass Rating
CDZ	Continuous Deformation zone
ALP	Adriyala Longwall Project
MPR	Maximum Pressure Recovery
MLR	Multiple Linear Regression
SF	Stability Factor Of The Pillar
SVM	Support Vector Machine
SVR	Support Vector Regression
RBF	Radial Basis Function

VAF	Variance Account For
MAPE	Mean Absolute Percentage Error
RMSE	Root Mean Square Error